

CSI 5138: Homework 4

Narmadha Sambandam, 300098713 Dharna Shukla, 300051861

Nov 14, 2019

Variational Autoencoders:

This section discusses the results of the implementation of the Variational Autoencoders (VAE) model trained on MNIST and CIFAR10 datasets using reference [?]. The two key hyper-parameters, latent space dimension as well as model complexity were investigated. In the context of VAE, the model complexity is defined as the intermediate dimension representing the dimension of the dense layer receiving the input.

Varying latent space dimension:

The first case tested was with the intermediate dimension remaining fixed at 512 with varying latent dimensions 2, 5, and 10. It was noticed that this did not contribute to any improvement in training time since it took about the same run time per epoch regardless of the latent dimensions used.

Given below is the plot of the loss function for VAE with intermediate dimension at 512 with varying latent dimensions 2, 5, and 10 for MNIST and CEFAR-10. It can be observed both training and test loss decreases as the latent space increases.

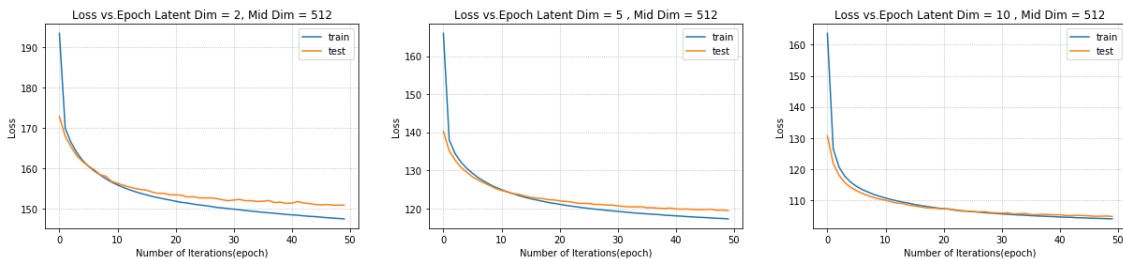


Figure 1: Plot of the loss function for VAE for MNIST

Compared to MNIST, the losses are much higher for CIFAR-10 where the loss are in the thousands vs. the hundreds on MNIST. A possible reason for this is that CIFAR-10 is more complex dataset than MNIST. Note, the erratic nature of the test curve could be a result of dataset allocating only 10,000 sample data for the test set as opposed to 50,000 for the train set.

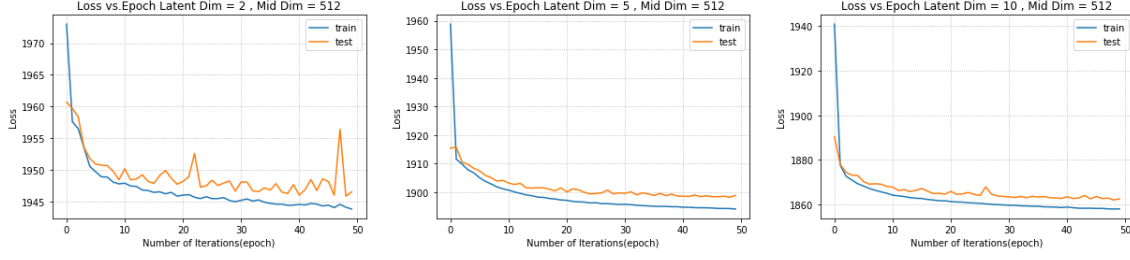
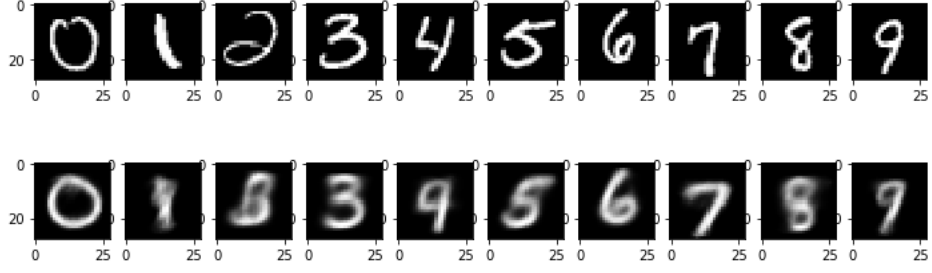
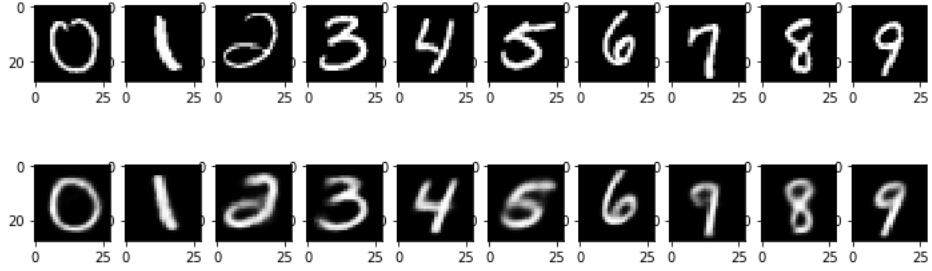


Figure 2: Plot of the loss function for VAE for CIFAR-10

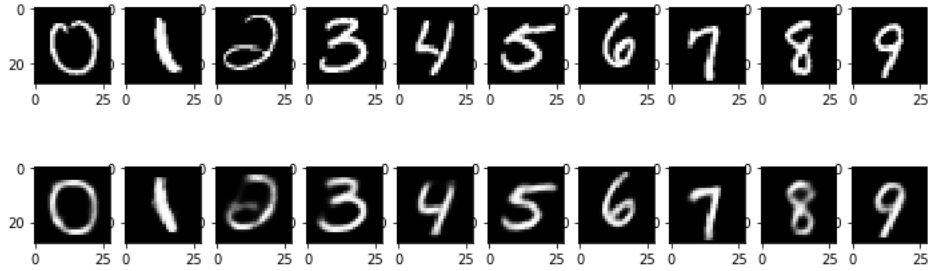
Given below are the generated images for VAE with intermediate dimension at 512 with varying latent dimensions 2, 5, and 10 for MNIST and CIFAR-10. Overall, larger latent dimensions yielded in a better quality for the generated images. The generated images in (c) resulted in the least blurry images with a corresponding latent dimension 10. The reason for the reconstruction being blurry is because the input is compressed at the bottleneck (latent space) layer which is controlled by its dimension. Hence, it is sensible that a larger latent dimension yields a higher quality.



(a) Original (top) vs generated images for VAE for MNIST with intermediate dimension at 512 with latent dimension 2 (bottom)



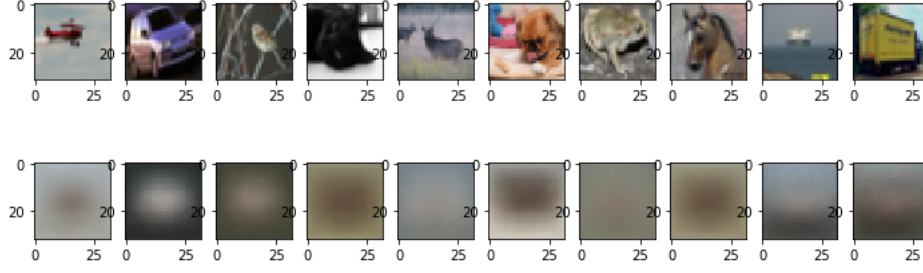
(b) Original (top) vs generated images for VAE for MNIST with intermediate dimension at 512 with latent dimension 5 (bottom)



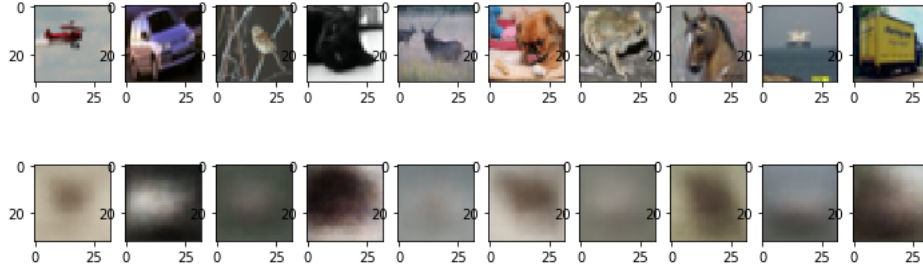
(c) Original (top) vs generated images for VAE for MNIST with intermediate dimension at 512 with latent dimension 10 (bottom)

Figure 3: Plot of the generated images for VAE for MNIST

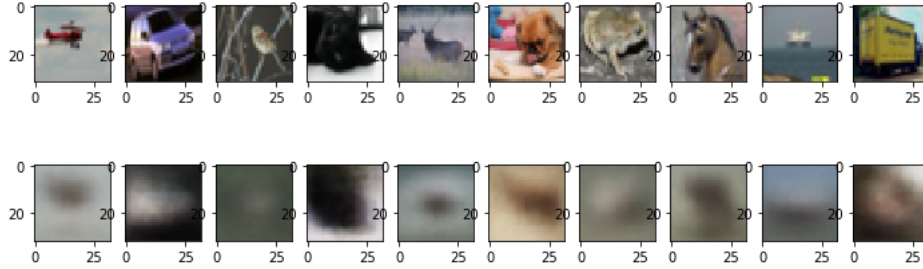
The higher losses of the CEFAR-10 dataset is indicative of the poorly generated images which are barely legible. Although the objects are too blurry to identify in the images, the larger latent dimension makes it possible to relate the generated images to the original based on the colour scheme and the low visibility of the outline of the object.



(a) Original (top) vs generated images for VAE for CEFAR-10 with intermediate dimension at 512 with latent dimension 2 (bottom)



(b) Original (top) vs generated images for VAE for CEFAR-10 with intermediate dimension at 512 with latent dimension 5 (bottom)



(c) Original (top) vs generated images for VAE for CEFAR-10 with intermediate dimension at 512 with latent dimension 10 (bottom)

Figure 4: Plot of the generated images for VAE for CEFAR-10

Varying model complexity:

While keeping the latent dimension fixed at 2, the model complexity was varied by modifying the intermediate dimension to 128, 256 and 512. As expected, the run time was much faster per epoch for the smaller intermediate dimensions.

Given below is the plot of the loss function for VAE with latent dimension at 2 with varying intermediate dimensions 128, 256 and 512 for MNIST and CEFAR-10. It can be observed that loss converges more quickly with larger intermediate dimensions. However, the divergence in loss

between the train and test sets increase with larger dimensions.

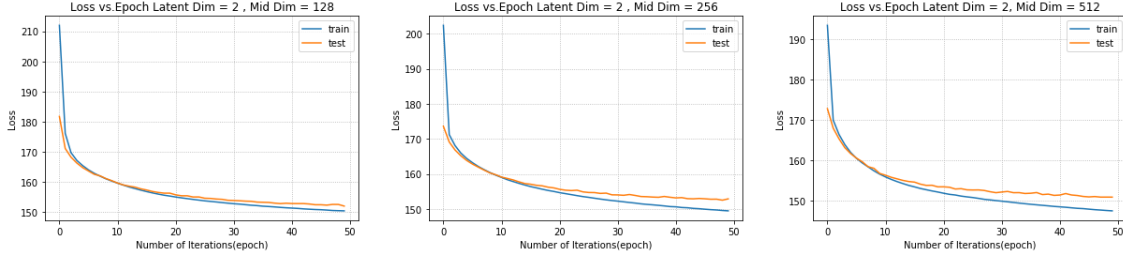


Figure 5: Plot of the loss function for VAE for MNIST

The losses are higher as expected for CEFAR-10 as previously discussed in the test for latent space dimensionality. Similar to MNIST, the losses converge quicker with larger intermediate dimensions. Note, the erratic nature of the test curve could be a result of dataset allocating only 10,000 sample data for the test set as opposed to 50,000 for the train set.

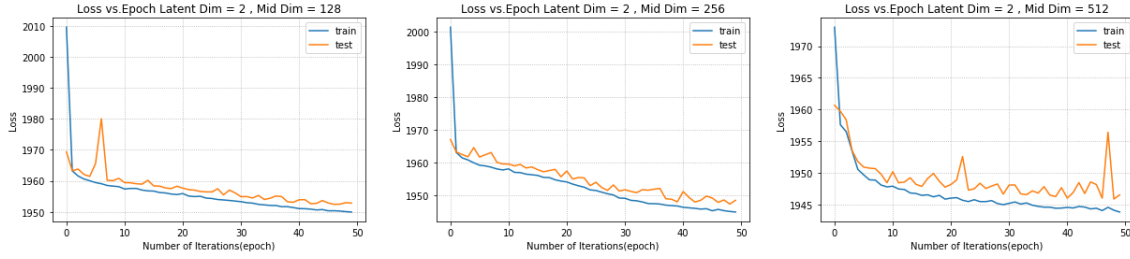
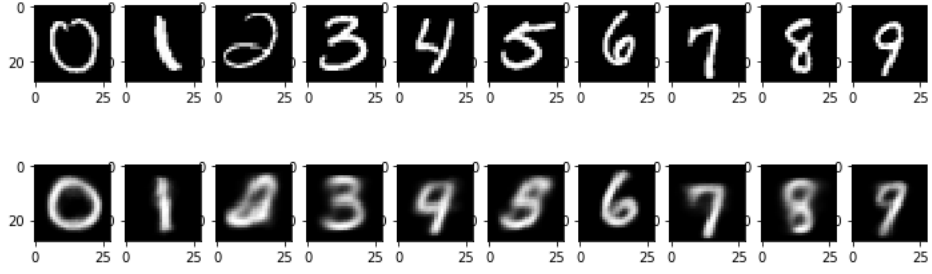


Figure 6: Plot of the loss function for VAE for CEFAR-10

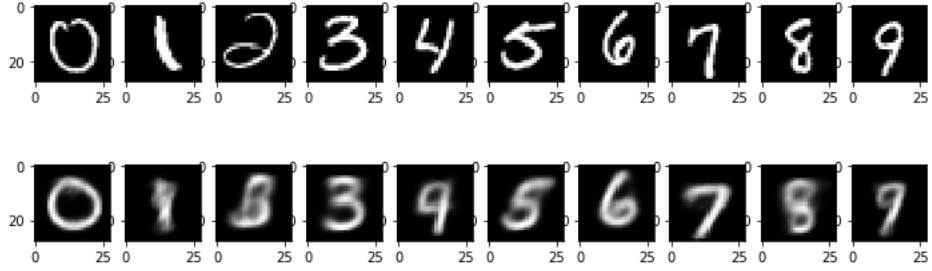
Given below are the generated images for VAE with latent dimension at 2 with varying intermediate dimensions 128, 256 and 512 for MNIST and CEFAR-10. It can be seen that larger intermediate dimension did not yield in a better quality images. In both datasets, the generated images are remain blurry despite any changes to the intermediate dimensionality.



(a) Original (top) vs generated images for VAE for MNIST with intermediate dimension at 128 with latent dimension 2 (bottom)

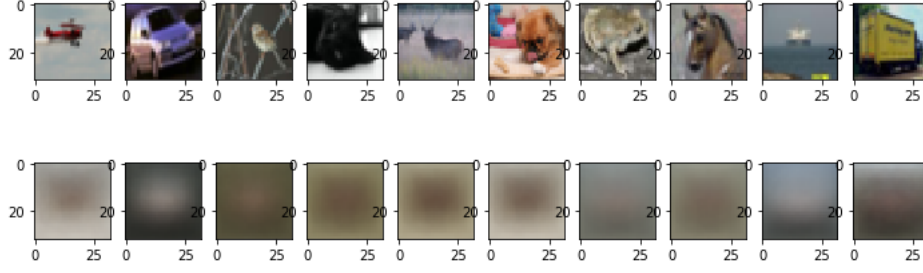


(b) Original (top) vs generated images for VAE for MNIST with intermediate dimension at 256 with latent dimension 2 (bottom)

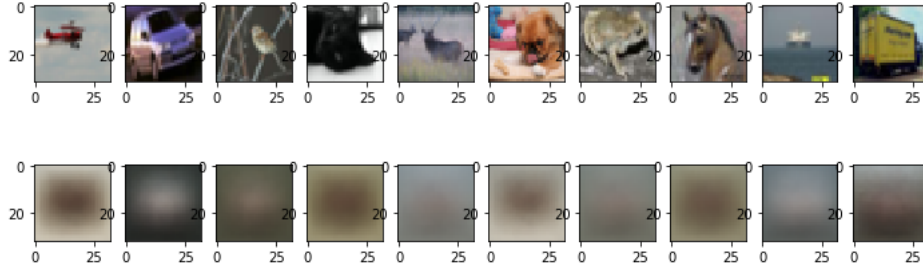


(c) Original (top) vs generated images for VAE for MNIST with intermediate dimension at 512 with latent dimension 2 (bottom)

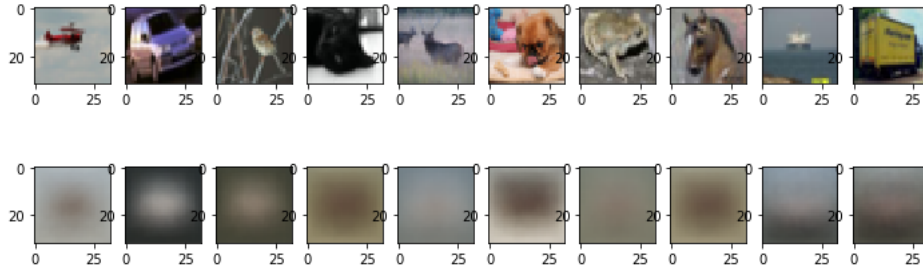
Figure 7: Plot of the generated images for VAE for MNIST



(a) Original (top) vs generated images for VAE for CIFAR-10 with intermediate dimension at 512 with latent dimension 2 (bottom)



(b) Original (top) vs generated images for VAE for CIFAR-10 with intermediate dimension at 512 with latent dimension 5 (bottom)



(c) Original (top) vs generated images for VAE for CIFAR-10 with intermediate dimension at 512 with latent dimension 10 (bottom)

Figure 8: Plot of the generated images for VAE for CIFAR-10

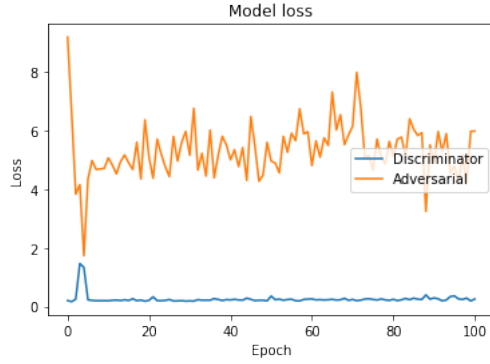
Generative Adversarial Network:

This section discusses the results of the implementation of the Generative Adversarial Network (GAN) model trained on MNIST and CIFAR10 datasets using reference. The two key hyper-parameters, latent space dimension as well as model complexity were investigated. The model complexity is defined as the intermediate dimension representing the dimension of the dense layers receiving the input. As vanilla GANs are rather unstable, an alternate is the Deep Convolution GAN (DCGAN) model which contain features like convolutional layers and batch normalization which can help with

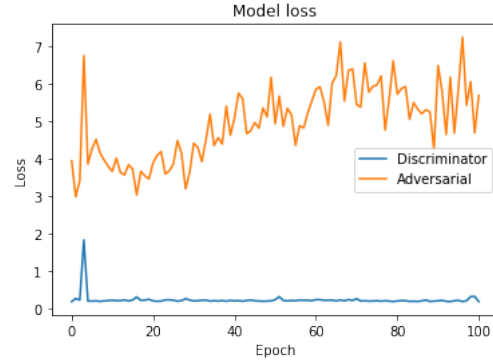
the stability of the convergence.

Varying latent space dimension:

As shown below in the model loss plot, there was no considerable change in the JSD loss when the latent dimension was modified from 100 to 10. Both discriminator and generator losses eventually oscillate over some optimum found by the GAN model, where it can't improve more, which also should mean that it has learned well enough.

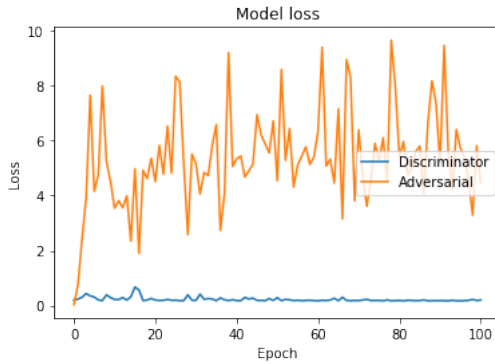


(a) Plot of model losses with latent dimension 100 for MNIST

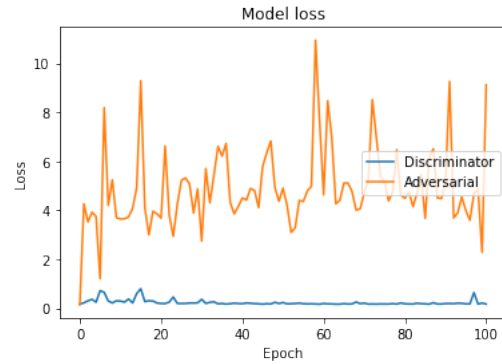


(b) Plot of model losses with latent dimension 10 for MNIST

Figure 9: Plot of the model loss for DCGAN for MNIST



(a) Plot of model losses with latent dimension 100 for CIFAR-10



(b) Plot of model losses with latent dimension 10 for CIFAR-10

Figure 10: Plot of the model loss for DCGAN for CIFAR-10

Given below are the generated images for DCGAN with latent dimensions 100 and 10 for MNIST and CIFAR-10. As expected, it can be seen that the images are not visually differentiable in terms

of their resolutions. It is easier to tell for the MNIST dataset but harder for CIFAR-10 since the images are more complex.

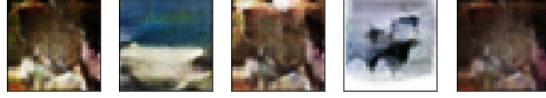


(a) Generated images with latent dimension 100 for MNIST



(b) Generated images with latent dimension 10 for MNIST

Figure 11: Generated images for DCGAN for MNIST



(a) Generated images with latent dimension 100 for CIFAR-10



(b) Generated images with latent dimension 10 for CIFAR-10

Figure 12: Generated images for DCGAN for CIFAR-10

Varying model complexity:

In the case of DCGAN, modifying the model complexity can impact the performance of the model. Having rather larger dense layer accepting the generator input can lead to the generator creating the same output always, no matter what the input noise (mode collapse). In such a scenario, the generator will never be directly incentivised to cover all modes. Thus, the generator will exhibit very poor diversity amongst generated samples, which limits the usefulness of the learnt GAN. On the other hand, not using a dense layer at all can lead to the generator not learning anything meaningful after many iterations. We can reach certain bottleneck that increasing the complexity of the generator does not necessarily improve the image quality. Figure 26 and 14 shows two architecture implemented where one implements deeper layers than the other. Although the initial iteration generated more realistic images with the deeper architecture (Figure 15 and 16), the final generated images resemble each other as shown in Figure 17 and 18.

Layer (type)	Output Shape	Param #
dense_1 (Dense)	(None, 6272)	633472
reshape_1 (Reshape)	(None, 7, 7, 128)	0
conv2d_transpose_1 (Conv2DTr	(None, 14, 14, 64)	73792
batch_normalization_1 (Batch	(None, 14, 14, 64)	256
re_lu_1 (ReLU)	(None, 14, 14, 64)	0
conv2d_transpose_2 (Conv2DTr	(None, 14, 14, 32)	18464
batch_normalization_2 (Batch	(None, 14, 14, 32)	128
re_lu_2 (ReLU)	(None, 14, 14, 32)	0
conv2d_transpose_3 (Conv2DTr	(None, 28, 28, 1)	289
Total params: 726,401		
Trainable params: 726,209		
Non-trainable params: 192		

(a) Architecture 1: An effective DCGAN generator architecture for MNIST

Layer (type)	Output Shape	Param #
dense_4 (Dense)	(None, 12544)	1266944
reshape_4 (Reshape)	(None, 7, 7, 256)	0
conv2d_transpose_8 (Conv2DTr	(None, 14, 14, 128)	295040
batch_normalization_6 (Batch	(None, 14, 14, 128)	512
re_lu_6 (ReLU)	(None, 14, 14, 128)	0
conv2d_transpose_9 (Conv2DTr	(None, 14, 14, 64)	73792
batch_normalization_7 (Batch	(None, 14, 14, 64)	256
re_lu_7 (ReLU)	(None, 14, 14, 64)	0
conv2d_transpose_10 (Conv2DT	(None, 28, 28, 1)	577
Total params: 1,637,121		
Trainable params: 1,636,737		
Non-trainable params: 384		

(b) Architecture 2: Deeper DCGAN generator architecture for MNIST

Figure 13: Architectures explored for DCGAN for MNIST

Layer (type)	Output Shape	Param #
dense_1 (Dense)	(None, 2048)	206848
reshape_1 (Reshape)	(None, 2, 2, 512)	0
batch_normalization_1 (Batch Normalization)	(None, 2, 2, 512)	2048
leaky_re_lu_1 (LeakyReLU)	(None, 2, 2, 512)	0
conv2d_transpose_1 (Conv2DTr)	(None, 4, 4, 256)	3277056
batch_normalization_2 (Batch Normalization)	(None, 4, 4, 256)	1024
leaky_re_lu_2 (LeakyReLU)	(None, 4, 4, 256)	0
conv2d_transpose_2 (Conv2DTr)	(None, 8, 8, 128)	819328
batch_normalization_3 (Batch Normalization)	(None, 8, 8, 128)	512
leaky_re_lu_3 (LeakyReLU)	(None, 8, 8, 128)	0
conv2d_transpose_3 (Conv2DTr)	(None, 16, 16, 64)	204864
batch_normalization_4 (Batch Normalization)	(None, 16, 16, 64)	256
leaky_re_lu_4 (LeakyReLU)	(None, 16, 16, 64)	0
conv2d_transpose_4 (Conv2DTr)	(None, 32, 32, 3)	4803
Total params: 4,516,739		
Trainable params: 4,514,819		
Non-trainable params: 1,920		

(a) Architecture 1: An effective DCGAN generator architecture for CIFAR-10

Layer (type)	Output Shape	Param #
dense_3 (Dense)	(None, 4096)	413696
reshape_3 (Reshape)	(None, 2, 2, 1024)	0
batch_normalization_9 (Batch Normalization)	(None, 2, 2, 1024)	4096
leaky_re_lu_9 (LeakyReLU)	(None, 2, 2, 1024)	0
conv2d_transpose_9 (Conv2DTr)	(None, 4, 4, 512)	13107712
batch_normalization_10 (Batch Normalization)	(None, 4, 4, 512)	2048
leaky_re_lu_10 (LeakyReLU)	(None, 4, 4, 512)	0
conv2d_transpose_10 (Conv2DTr)	(None, 8, 8, 256)	3277056
batch_normalization_11 (Batch Normalization)	(None, 8, 8, 256)	1024
leaky_re_lu_11 (LeakyReLU)	(None, 8, 8, 256)	0
conv2d_transpose_11 (Conv2DTr)	(None, 16, 16, 128)	819328
batch_normalization_12 (Batch Normalization)	(None, 16, 16, 128)	512
leaky_re_lu_12 (LeakyReLU)	(None, 16, 16, 128)	0
conv2d_transpose_12 (Conv2DTr)	(None, 32, 32, 3)	9603
Total params: 17,635,075		
Trainable params: 17,631,235		
Non-trainable params: 3,840		

(b) Architecture 2: Deeper DCGAN generator architecture for CIFAR-10

Figure 14: Architectures explored for DCGAN for CIFAR-10

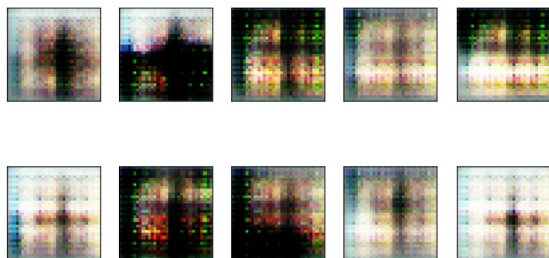


(a) Generated images after first iteration for Architecture 1 for MNIST

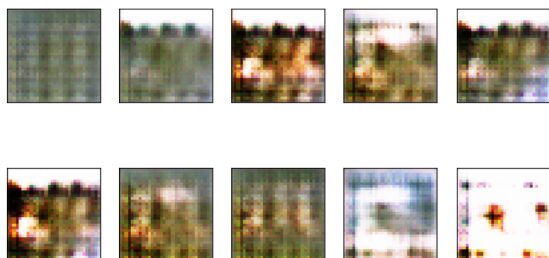


(b) Generated images after first iteration for Architecture 2 for MNIST

Figure 15: Generated images of architectures explored for DCGAN for MNIST



(a) Generated images after first iteration for Architecture 1 for CIFAR-10



(b) Generated images after first iteration for Architecture 2 for CIFAR-10

Figure 16: Generated images of architectures explored for DCGAN for CIFAR-10

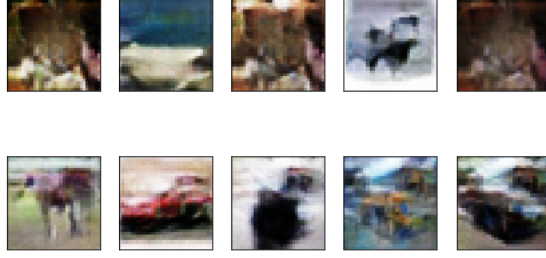


(a) Generated images after final iteration for Architecture 1 for MNIST



(b) Generated images after final iteration for Architecture 2 for MNIST

Figure 17: Generated images of architectures explored for DCGAN for MNIST



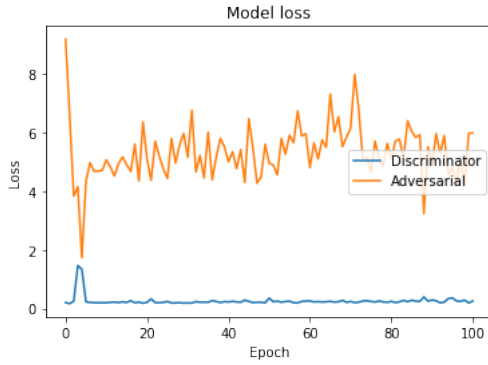
(a) Generated images after final iteration for Architecture 1 for CIFAR-10



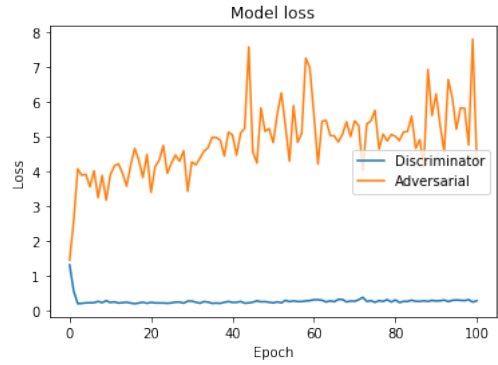
(b) Generated images after final iteration for Architecture 2 for CIFAR-10

Figure 18: Generated images of architectures explored for DCGAN for CIFAR-10

The corresponding loss curves for both architectures are given below.

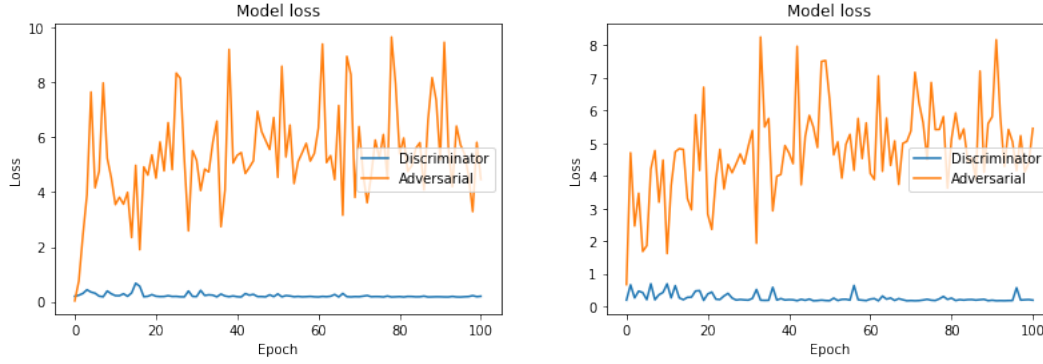


(a) Plot of model losses with Architecture 1 for MNIST



(b) Plot of model losses with Architecture 2 for MNIST

Figure 19: Plot of the model loss for DCGAN for MNIST



(a) Plot of model losses with Architecture 1 for CIFAR-10

(b) Plot of model losses with Architecture 2 for CIFAR-10

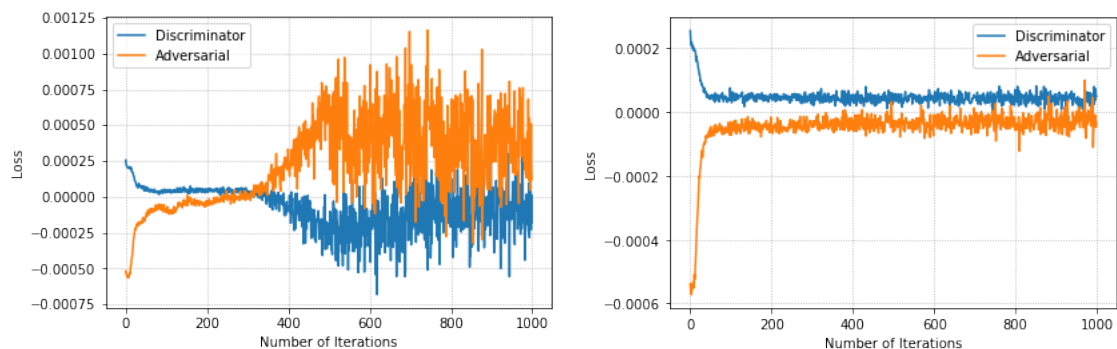
Figure 20: Plot of the model loss for DCGAN for CIFAR-10

Wasserstein Generative Adversarial Network:

The goal of WGAN is to better stabilize GAN training and diminish some disadvantages of other GAN models such as mode collapse and uninformative loss. Thus, WGAN was implemented with properties such as a meaningful loss metric to correlate generator's convergence and quality of samples. Also, it can improve the overall stability of the optimization process.

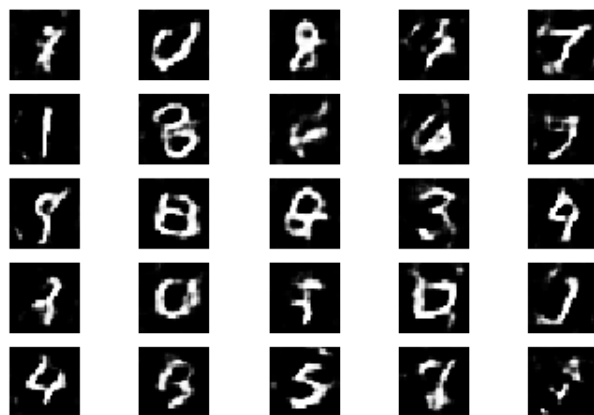
Varying latent space dimension:

Given below is the estimated EMD loss of WGAN with latent dimensions 100 and 10. We find the loss starts converging after 600 epoch for latent space of 100. In the case of the smaller dimension, the loss converges faster. More training seems to result in better quality generated images especially after reaching a state of convergence the quality remains about the same for the model.

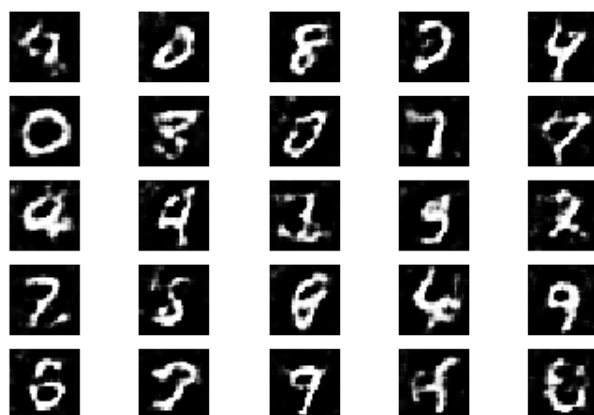


(a) Plot of model losses with latent dimension 100 for MNIST
(b) Plot of model losses with latent dimension 10 for MNIST

Figure 21: Plot of the model loss for WGAN for MNIST

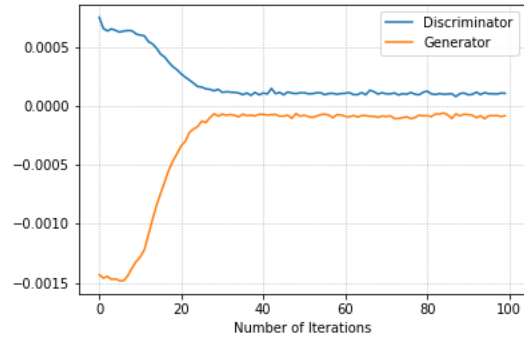


(a) Generated images with latent dimension 100 for MNIST

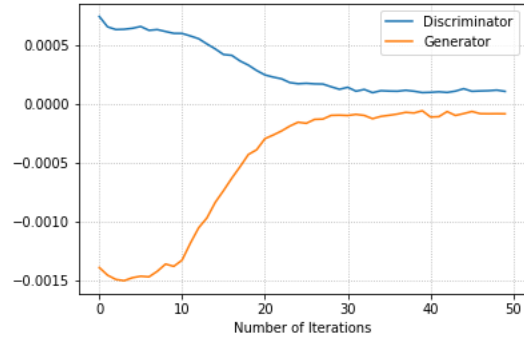


(b) Generated images with latent dimension 10 for MNIST

Figure 22: Generated images for WGAN for MNIST

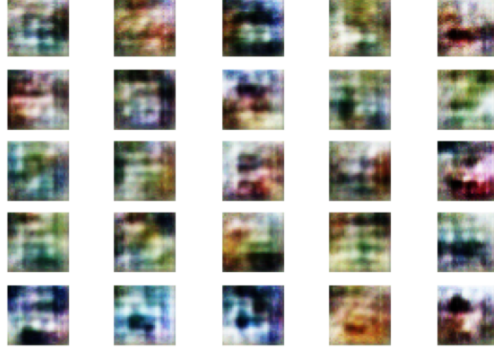


(a) Plot of model losses with latent dimension 100 for CIFAR-10

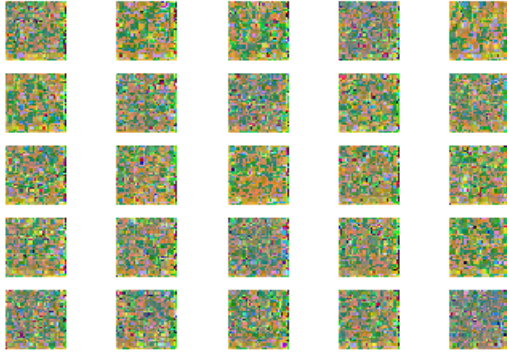


(b) Plot of model losses with latent dimension 10 for CIFAR-10

Figure 23: Plot of the model loss for WGAN for CIFAR-10



(a) Generated images with latent dimension 100 for CIFAR-10



(b) Generated images with latent dimension 10 for CIFAR-10

Figure 24: Generated images for WGAN for CIFAR-10

Varying model complexity:

After testing numerous model architecture, the two that are given below are chosen to demonstrate for comparison purposes. The deeper architecture did improve the generated images to create more plausible digits. If the architecture is too simple, the fabricated images remained more like noise. Although the difference is small, the images generated after first 50 epoch with the deeper architecture are preliminary stages of forming edges. With continued tuning of the complexity, it maybe possible to improve results further. CIFAR-10 is a more complex dataset thus the model requires larger number of iterations to generate more realistic looking images than what was explored in the assignment.

Layer (type)	Output Shape	Param #
=====	=====	=====
dense_2 (Dense)	(None, 6272)	633472
reshape_1 (Reshape)	(None, 7, 7, 128)	0
up_sampling2d_1 (UpSampling2D)	(None, 14, 14, 128)	0
conv2d_5 (Conv2D)	(None, 14, 14, 64)	131136
batch_normalization_4 (Batch Normalization)	(None, 14, 14, 64)	256
activation_1 (Activation)	(None, 14, 14, 64)	0
up_sampling2d_2 (UpSampling2D)	(None, 28, 28, 64)	0
conv2d_6 (Conv2D)	(None, 28, 28, 32)	32800
batch_normalization_5 (Batch Normalization)	(None, 28, 28, 32)	128
activation_2 (Activation)	(None, 28, 28, 32)	0
conv2d_7 (Conv2D)	(None, 28, 28, 1)	513
activation_3 (Activation)	(None, 28, 28, 1)	0
=====	=====	=====
Total params: 798,305		
Trainable params: 798,113		
Non-trainable params: 192		

(a) Architecture 1: An effective WGAN generator architecture for MNIST

Layer (type)	Output Shape	Param #
=====	=====	=====
dense_2 (Dense)	(None, 12544)	1266944
reshape_1 (Reshape)	(None, 7, 7, 256)	0
up_sampling2d_1 (UpSampling2D)	(None, 14, 14, 256)	0
conv2d_5 (Conv2D)	(None, 14, 14, 128)	524416
batch_normalization_4 (Batch Normalization)	(None, 14, 14, 128)	512
activation_1 (Activation)	(None, 14, 14, 128)	0
up_sampling2d_2 (UpSampling2D)	(None, 28, 28, 128)	0
conv2d_6 (Conv2D)	(None, 28, 28, 64)	131136
batch_normalization_5 (Batch Normalization)	(None, 28, 28, 64)	256
activation_2 (Activation)	(None, 28, 28, 64)	0
conv2d_7 (Conv2D)	(None, 28, 28, 1)	1025
activation_3 (Activation)	(None, 28, 28, 1)	0
=====	=====	=====
Total params: 1,924,289		
Trainable params: 1,923,905		
Non-trainable params: 384		

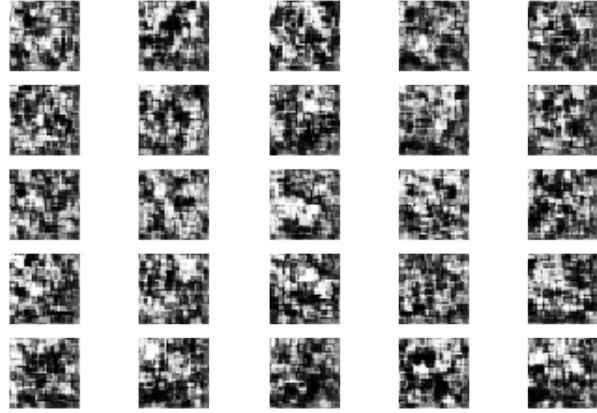
(b) Architecture 2: Deeper WGAN generator architecture for MNIST

Figure 25: Architectures explored for WGAN for MNIST

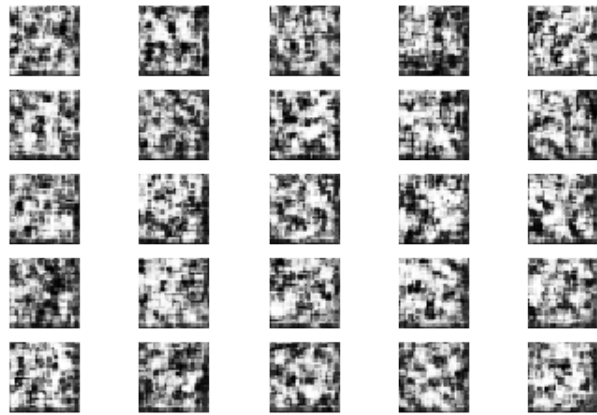
Layer (type)	Output Shape	Param #
conv2d_6 (Conv2D)	(None, 16, 16, 16)	448
leaky_re_lu_3 (LeakyReLU)	(None, 16, 16, 16)	0
dropout_3 (Dropout)	(None, 16, 16, 16)	0
conv2d_7 (Conv2D)	(None, 8, 8, 256)	37120
zero_padding2d_1 (ZeroPaddin	(None, 9, 9, 256)	0
batch_normalization_4 (Batch	(None, 9, 9, 256)	1024
leaky_re_lu_4 (LeakyReLU)	(None, 9, 9, 256)	0
dropout_4 (Dropout)	(None, 9, 9, 256)	0
conv2d_8 (Conv2D)	(None, 9, 9, 1024)	2360320
batch_normalization_5 (Batch	(None, 9, 9, 1024)	4096
leaky_re_lu_5 (LeakyReLU)	(None, 9, 9, 1024)	0
dropout_5 (Dropout)	(None, 9, 9, 1024)	0
flatten_1 (Flatten)	(None, 82944)	0
dense_2 (Dense)	(None, 1)	82945
Total params: 2,485,953		
Trainable params: 2,483,393		
Non-trainable params: 2,560		

(a) Architecture 1: An effective WGAN generator architecture for CIFAR-10

Layer (type)	Output Shape	Param #
conv2d_22 (Conv2D)	(None, 16, 16, 16)	448
leaky_re_lu_12 (LeakyReLU)	(None, 16, 16, 16)	0
dropout_10 (Dropout)	(None, 16, 16, 16)	0
conv2d_23 (Conv2D)	(None, 8, 8, 128)	18560
zero_padding2d_2 (ZeroPaddin	(None, 9, 9, 128)	0
batch_normalization_18 (Batc	(None, 9, 9, 128)	512
leaky_re_lu_13 (LeakyReLU)	(None, 9, 9, 128)	0
dropout_11 (Dropout)	(None, 9, 9, 128)	0
conv2d_24 (Conv2D)	(None, 5, 5, 256)	295168
batch_normalization_19 (Batc	(None, 5, 5, 256)	1024
leaky_re_lu_14 (LeakyReLU)	(None, 5, 5, 256)	0
dropout_12 (Dropout)	(None, 5, 5, 256)	0
conv2d_25 (Conv2D)	(None, 3, 3, 512)	1180160
batch_normalization_20 (Batc	(None, 3, 3, 512)	2048
leaky_re_lu_15 (LeakyReLU)	(None, 3, 3, 512)	0
dropout_13 (Dropout)	(None, 3, 3, 512)	0
conv2d_26 (Conv2D)	(None, 3, 3, 1024)	4719616
batch_normalization_21 (Batc	(None, 3, 3, 1024)	4096
leaky_re_lu_16 (LeakyReLU)	(None, 3, 3, 1024)	0
conv2d_27 (Conv2D)	(None, 3, 3, 1024)	9438208
batch_normalization_22 (Batc	(None, 3, 3, 1024)	4096
leaky_re_lu_17 (LeakyReLU)	(None, 3, 3, 1024)	0
dropout_14 (Dropout)	(None, 3, 3, 1024)	0
flatten_2 (Flatten)	(None, 9216)	0
dense_4 (Dense)	(None, 1)	9217

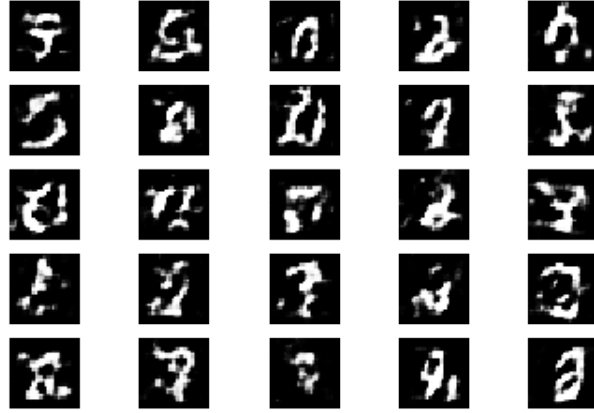


(a) Generated images with Architecture 1 for MNIST after initial 50 epoch

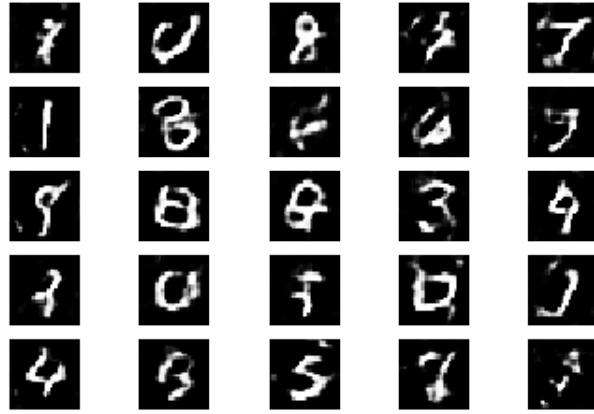


(b) Generated images with Architecture 2 for MNIST after initial 50 epoch

Figure 27: Generated images for WGAN for MNIST

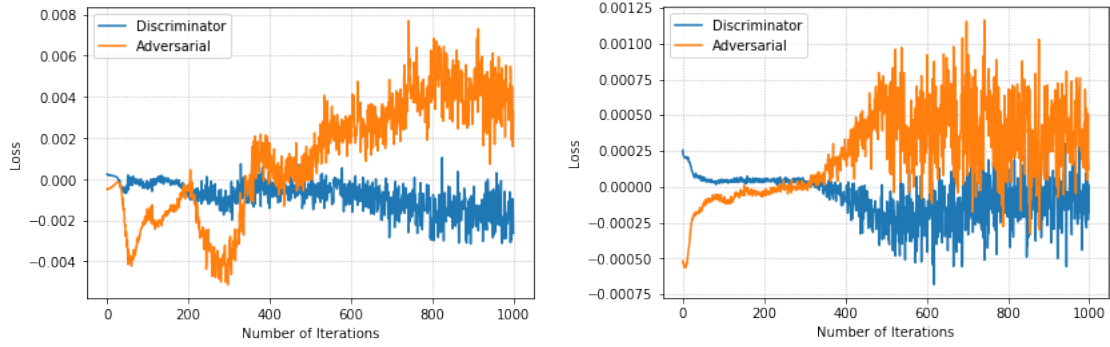


(a) Generated images with Architecture 1 for MNIST after final epoch



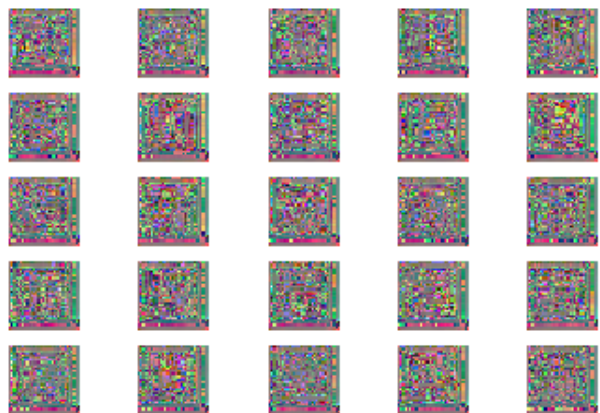
(b) Generated images with Architecture 2 for MNIST after final epoch

Figure 28: Generated images for WGAN for MNIST

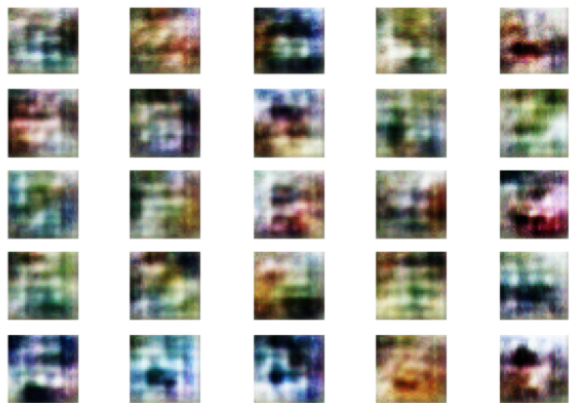


(a) Plot of model losses with Architecture 1 for MNIST (b) Plot of model losses with Architecture 2 for MNIST

Figure 29: Plot of the model loss for WGAN for MNIST

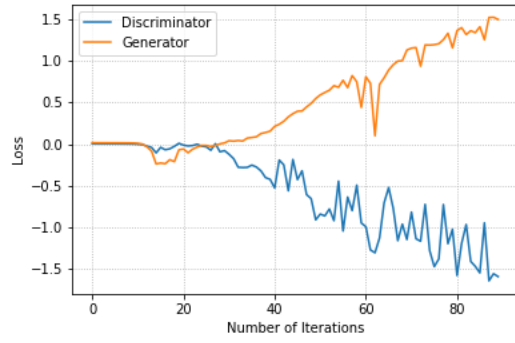


(a) Generated images with Architecture 1 for CIFAR-10 after final epoch

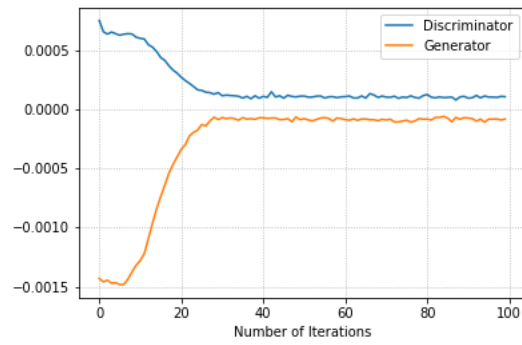


(b) Generated images with Architecture 2 for CIFAR-10 after final epoch

Figure 30: Generated images for WGAN for CIFAR-10



(a) Plot of model losses with Architecture 1 for CIFAR-10



(b) Plot of model losses with Architecture 1 for CIFAR-10

Figure 31: Plot of the model loss for WGAN for CIFAR-10